Kinetic Effects in Relativistic Shocks

A. Stockem[1], *R.A. Fonseca*[12], *L.O. Silva*[1]

[1]*IPFN, IST, Lisbon, Portugal,* [2]*DCTI, ISCTE - Lisbon University Institute Portugal*

The formation and generation of shocks is a topic of wide interest in many fields of physics, but the role of the kinetic effects and the properties of the particle distribution function across the shock front have not been explored in detail. Using particle-in-cell simulations to study electron-positron collisionless shocks we explore the features of the particle distribution in the upstream, downstream, and shock transition region, and the deviations to a Maxwellian distribution. The theoretical model developed to account for these effects shows that a strong tail can change the shock properties (shock velocity, jump conditions) significantly. However, in the standard case, the decrease of the upstream bulk speed has a bigger impact. These effects are illustrated with particle-in-cell simulations. The relevance of these results for astrophysical shocks is also discussed.

1 Introduction

The study of shocks has gained broad interest in the scientific community as they can provide an efficient particle acceleration, but our knowledge in this area is still very limited. Representatives of non-relativistic shocks are the super novae, which are a promising candidate inside our galaxy to accelerate cosmic rays to the observed ultra-high energies [1]. The explosions of gamma-ray bursts (GRBs), outflows of active galactic nuclei (AGNi) or pulsar wind nebulae (PWN) are representatives of relativistic shocks.

Also for medical applications shocks can play an important role as proton energies up to 250 MeV are needed which cannot be achieved by target normal sheath acceleration (TNSA). It has been found in simulations that proton shock acceleration (PSA) can produce quasi monoenergetic protons with very high energies [2]. The PSA process occurs in a different parameter regime, where a very thin target foil and very high laser intensities are necessary.

Two main models exist for the acceleration process in collisionless shocks, which are both based on the bouncing of the particles back and forth across the shock front. In the shock-drift acceleration process, the particles gain energy from the electric field when they gyrate across the shock front. Diffusive shock acceleration describes the stochastic scattering of the particles off the turbulent electromagnetic field.

After some time, the shock reaches a quasi-steady state and its macroscopic properties are usually derived from a magnetohydrodynamic (MHD) model. In the case of highly relativistic shocks, according to the standard model [3] the shock properties are determined by the upstream bulk speed and the downstream adiabatic constant only.

We investigate the structure of such a relativistic shock with theory and simulations. With current computational resources, we are able to look at the shock details and to analyze the deviations from the standard model. In particular, we focus on the shock compression ratio and identify the dominant microscopic quantities that determine the global shock structure. Furthermore, we investigate the non-thermal particles and their effect on the jump conditions.

The rest of the article is organized as follows: we start with a brief review of the hydrodynamical model in Section 2 and compare it with our particle-in-cell (PIC) simulations in Section 3; in Section 4 the main quantities that determine the jump conditions are identified; the results are summarized in Section 5.

2 Review of the hydrodynamical model

For the derivation of the jump conditions, it is assumed that the shock has reached a quasi-steady state. The propagating upstream flow has been compressed due to instabilities and the downstream region has formed, which is considered to be at rest in our model. In this frame, the shock propagates with a speed β_s. A sketch of this model is shown in Figure 1. When particles cross the shock front and propagate between the upstream and downstream regions, mass, momentum and energy are conserved. The conservation equations in the shock frame are given by

$$n_1 u_{1s} = n_2 u_{2s} \tag{1}$$

$$\gamma_{1s}\mu_1 = \gamma_{2s}\mu_2 \tag{2}$$

$$u_{1s}\mu_1 + \frac{p_1}{n_1 u_{1s}} = u_{2s}\mu_2 + \frac{p_2}{n_2 u_{2s}} \tag{3}$$

with $u_{is} = \gamma_{is}\beta_{is}$, where γ_{is} denotes the Lorentz factor, $\beta_{is} = v_{is}/c$ where v_{is} is the bulk velocity, n_i is the plasma rest frame density, and $\mu_i = 1 + (\Gamma_i - 1)p_i/\Gamma_i n_i$ is the specific enthalpy. The index $i = 1, 2$ labels the upstream and downstream components, respectively.

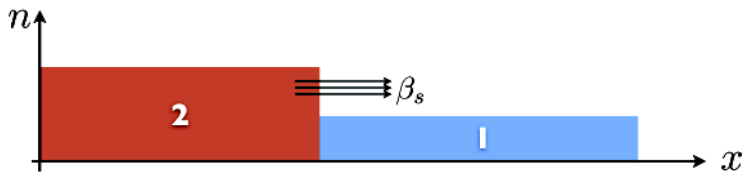

Figure 1: The upstream population in region 1 is compressed to higher densities, leading to the formation of downstream region 2, which is moving with the shock speed β_s.

In the case of a highly relativistic upstream the strong shock approximation $p_2/n_2 \gg p_1/n_1$ holds and we can apply $p_1 = e_1 = 0$. After performing a relativistic Lorentz transformation of Eqs. (1)-(3) into the downstream frame and using the relation between energy e_i and pressure density p_i that defines the adiabatic constant $\Gamma_i := 1 + p_i/(e_i - \rho_i)$ with rest mass density $\rho_i = n_i mc^2$, the jump conditions can be derived straight-forwardly. The shock velocity is given by

$$\beta_s = (\Gamma_2 - 1)\sqrt{\frac{\gamma_0 - 1}{\gamma_0 + 1}} \tag{4}$$

and the density compression ratio in the downstream frame is found to be

$$\frac{n_2}{n_1} = 1 + \frac{\beta_0}{\beta_s} = \frac{\Gamma_2}{\Gamma_2 - 1} + \frac{1}{\gamma_0(\Gamma_2 - 1)} \tag{5}$$

which both depend only on the upstream Lorentz factor γ_0 and the downstream adiabatic constant Γ_2 [4].

3 Simulations

In order to investigate the kinetic effects on the jump conditions, we perform two-dimensional particle-in-cell simulations with the fully relativistic code OSIRIS [5]. The initial setup is displayed in Fig. 2. The upstream flow consists of a charge-neutral beam of electrons and positrons and is injected with a cathode from the right wall with a Lorentz factor $\gamma_0 = 20$. The thermal velocity $v_{th} = 10^{-3}\,c$ is negligible. The shock is generated from a perfectly reflecting wall on the left-hand-side of the box. The initial number of particles per cell per

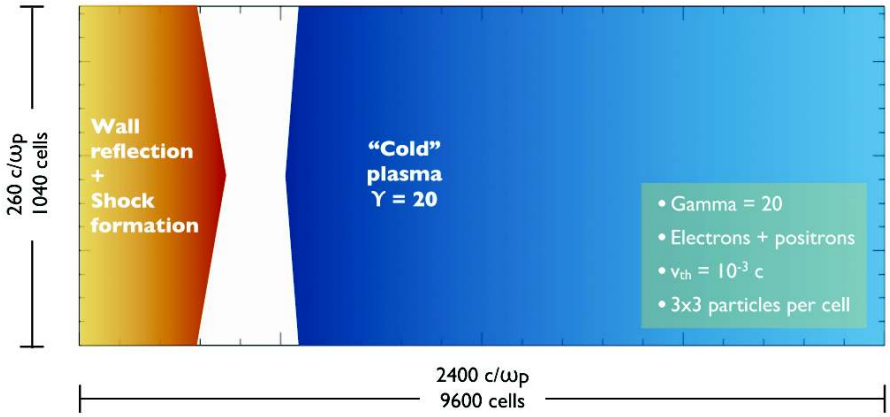

Figure 2: The upstream population of electrons and positrons is injected from the right wall. When the particles are reflected from the left wall, a shock is formed.

species is 9 and the box contains 1040×9600 cells with a cell size $\Delta x_1 = \Delta x_2 = 0.25\, c/\omega_{pe}$, electron frequency $\omega_{pe} = (4\pi n_0 e^2/m_e)^{1/2}$ and initial upstream density n_0.

Figure 3 shows a snapshot of the electron density for $t = 2395\, \omega_{pe}^{-1}$. The characteristic filamentary structure is visible, which is due to a Weibel-type instability. The averaged one-dimensional density shows the density jump from the upstream to the downstream, which matches with the theoretical prediction $n_2/n_1 = 3.1$ from Eq. (5). The theoretical prediction for the shock speed $\beta_s = 0.48$ from Eq. (4) also agrees well with the simulation result in Figure 4.

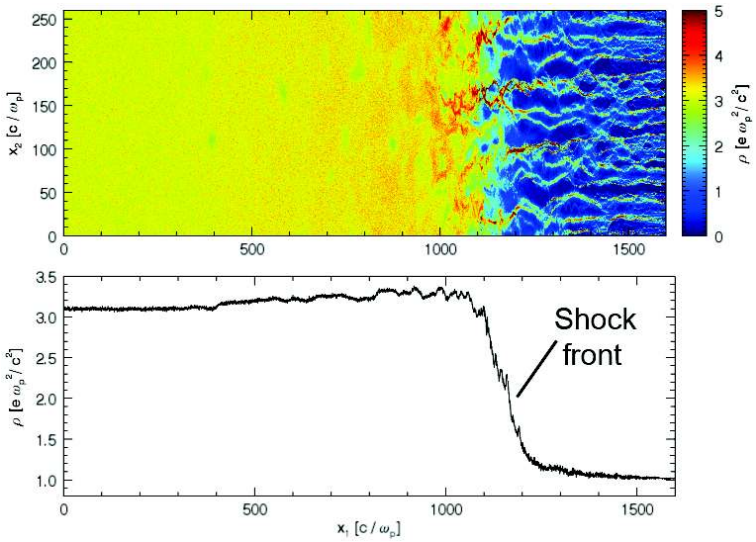

Figure 3: Two-dimensional electron density (top) and average over x_2 (bottom).

4 Identifying the critical parameters

The downstream particle spectra show a clear deviation from a thermal distribution and we first discuss the effect of a non-thermal tail on the jump conditions. We measure the energy and pressure densities

$$e \;:=\; \frac{\tilde{e}}{nmc^2} = \int d^3p\, \gamma\, f(\mathbf{p}) \tag{6}$$

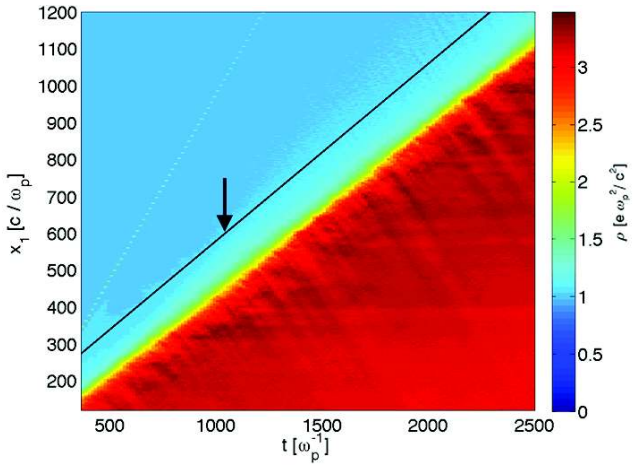

Figure 4: Plotting the density against x_1 and t allows to determine the shock speed. The theoretical prediction is given by the black line indicated by the arrow.

$$p \;:=\; \frac{\tilde{p}}{nmc^2} = \int d^3p\, \frac{p_x^2}{\gamma}\, f(\mathbf{p}) \tag{7}$$

with $\gamma = \sqrt{1+\mathbf{p}^2}$ directly from the simulation data and use the energy pressure relation to determine the real adiabatic constant. The obtained difference $\Delta\Gamma_2$ from the adiabatic constant of an ideal gas $\Gamma_2 = 3/2$ affects the density compression by

$$\Delta\left(n_2/n_1\right) \approx 4\Delta\Gamma_2, \tag{8}$$

which was obtained from a Taylor expansion of Eq. (5). The impact on the compression ratio can be strong if the adiabatic constant changes drastically. Moreover, we investigated the change of the density ratio n_2/n_1 depending on $\Delta\gamma_0$ and μ_1 if the assumption of a cold plasma is dropped. The deviation from the bulk Lorentz factor is defined as $\Delta\gamma_0 = \gamma_0 - \gamma_{12}$, where γ_{12} is the real Lorentz factor. Both, an increase in the adiabatic constant and in the upstream enthalpy lead to a decrease of the density compression, whereas an increase of $\Delta\gamma_0$ yields an increase of n_2/n_1.

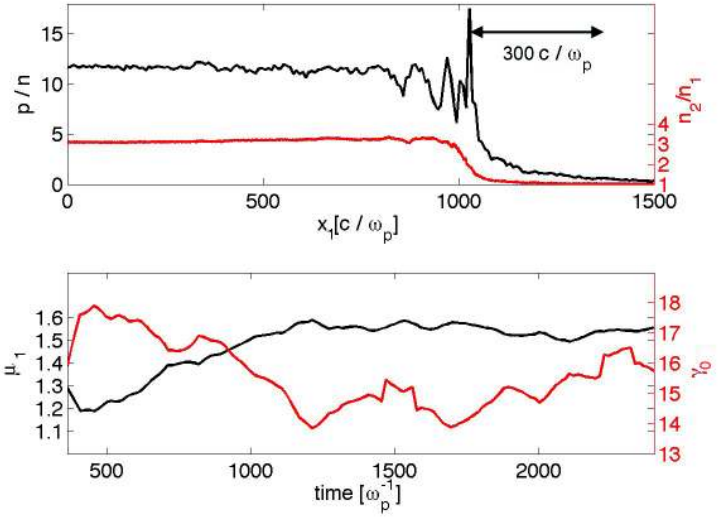

Figure 5: (a) Rest frame pressure and charge density ratio along x_1 for $t = 2273\,\omega_{pe}^{-1}$. (b) Specific enthalpy μ_1 and real bulk Lorentz factor γ_{12} directly ahead of the shock. The pressure peak is used as starting point for the integration over $300\,c/\omega_{pe}$.

Figure 5 shows the further parameters that we investigate to identify the relevant parameters that determine the structure of the shock. The peak in the pressure (Fig. 5a) is used to separate the downstream and upstream regions, as the density profile does not show a sharp transition. For the calculation of the bulk Lorentz factor γ_{12} and specific enthalpy μ_1 ahead of the shock, we have to define an integration range. The results shown here are for the range $300\, c/\omega_{pe}$. The temporal evolution of these two quantities is shown in Figure 5b and appears to be highly dynamic. The Lorentz factor deviates significantly from the initial upstream value $\gamma_0 = 20$.

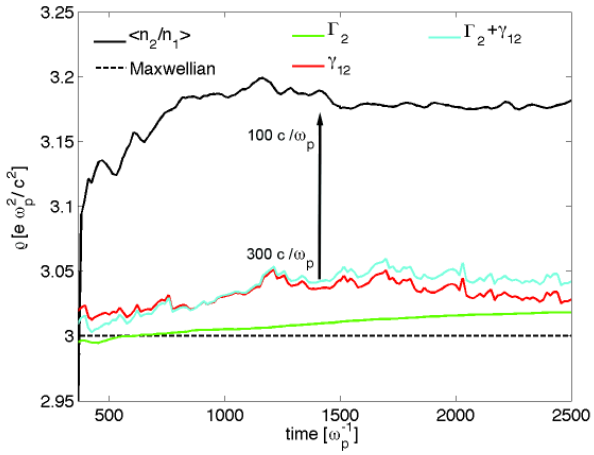

Figure 6: Downstream electron density from simulation data (solid black) and comparison with the theory.

The real quantities are applied to calculate the theoretical density ratio (Eq. 5), which is compared to the density ratio obtained from the simulation data, demonstrated in Fig. 6, and the particular contributions are discussed. The standard model with an unchanged upstream Lorentz factor $\gamma_0 = 20$ and a thermal downstream distribution provides a density ratio $n_2/n_1 = 3.0$, which differs significantly from the simulation data. Also, the consideration of a non-thermal downstream component that changes the adiabatic constant from $\Gamma_2 = 1.53$ to 1.52 at the end of the simulation, does not have a strong impact on the density ratio. The bulk Lorentz factor γ_{12} appears to be the significant parameter and we are able to match the simulation data with the theoretical model if the integration range is chosen to be $100\, c/\omega_{pe}$. Only particles in the vicinity of the shock front determine the shock parameters.

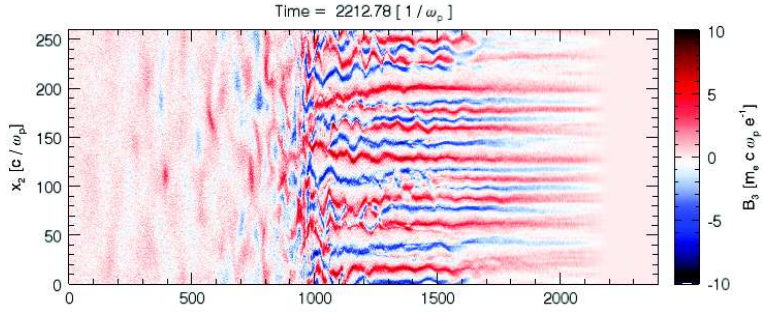

Figure 7: Self-consistently generated out of plane magnetic field.

Finally, we briefly mention the effect of electromagnetic fields on the jump conditions. From the simulations, we observe a self-consistently generated magnetic field component out of the plane (Fig. 7). If the conservation equations (1)-(3) are extended by the contribution of such a field, we find that it has a decreasing effect on the compression ratio n_2/n_1, which is of the order of 0.1 and explains the final decrease of the density ratio in Figure 6. Furthermore, we consider an initially magnetized plasma and the impact of a deviation in the adiabatic constant on the shock speed. We find that the effect is weaker as the initial magnetization $\sigma = B_0^2/4\pi n_0 \mu_1 \gamma_0^2$ gets stronger (Fig. 8).

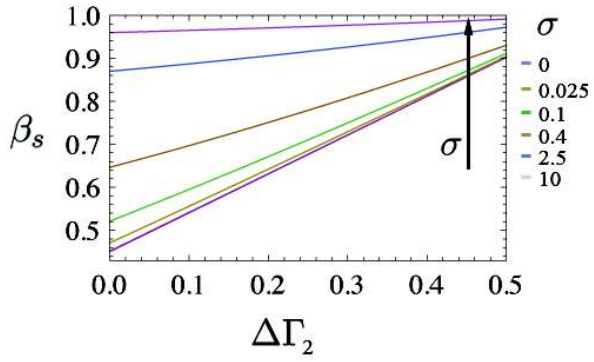

Figure 8: Dependence of the shock speed on the deviation of the adiabatic constant $\Delta\Gamma_2$ and initial magnetization σ.

5 Summary

We investigated the self-consistent generation of a shock in an initially unmagnetized plasma theoretically and with particle-in-cell simulations and determined the dominant parameters that determine the final structure of the shock. We found that the formation of a non-thermal particle component, with the associated decrease of the downstream adiabatic constant, and a decrease of the upstream Lorentz factor directly in front of the shock have an increasing effect on the shock compression ratio. The increase of the upstream pressure and the built-up of electromagnetic fields have a decreasing effect.

Our two-dimensional simulations show a deviation of 7% from the standard model for early simulation times. We identified the evolution of the upstream Lorentz factor in the vicinity of the shock front as the critical parameter with the largest effect on the jump conditions. For long propagation times, the contribution of the self-generated electromagnetic fields cannot be neglected, and it is responsible to maintain the quasi-steady state of the shock. Furthermore, the analysis allowed us to define a spatial range for the shock transition region, which we observed to be $100\, c/\omega_{pe}$.

Acknowledgments

AS acknowledges financial support from the Fundação para a Ciência e a Tecnologia (FCT) grant SFRH / BPD / 65008 / 2009. This work was also partially supported by the European Research Council (ERC-2010-AdG Grant 267841), and by FCT (Portugal) grants PTDC/FIS/111720/2009.

References

[1] CAPRIOLI, D., et al., "Non-linear Diffusive Acceleration of Heavy Nuclei in Supernova Remnant Shocks", Astroparticle Physics **34** (2011) 447

[2] SILVA, L.O., et al., "Proton Shock Acceleration in Laser-Plasma Interactions", Phys. Rev. Lett. **92** (2004) 015002

[3] BLANDFORD, R.D. and McKEE, C.F., "Fluid Dynamics of Relativistic Blast Waves", Phys. Fluids **19** (1976) 1130

[4] SPITKOVSKY, A., "On the Structure of Relativistic Collisionless Shocks in Electron-Ion Plasmas", Astrophys. J. **673** (2008) L39

[5] FONSECA, R.A., et al., "Osiris: a Three-dimensional Fully Relativistic Particle in Cell Code for Modeling Plasma based Accelerators", Lect. Notes Comput. Sci. **2331** (2002) 342